

RESONANCE PHENOMENA AND LONG-TERM CHAOTIC ADVECTION IN STOKES FLOWS

A Thesis
Submitted to
the Temple University Graduate Board

In Partial Fulfillment
of the Requirements for the Degree
MASTER OF SCIENCE IN ENGINEERING

By
Alimu Abudu
January, 2011

Dr. Dmitri Vainchtein, Thesis Advisor, Department of Mechanical
Engineering, Temple University

Dr. Richard Cohen, Committee Member, Department of Mechanical
Engineering, Temple University

Dr. Chang-Hee Won, Committee Member, Department of Electrical
and Computer Engineering, Temple University

ABSTRACT

Title: Resonance Phenomena and Long-term Chaotic Advection in Stokes Flows

Candidate's name: Alimu Abudu

Degree: Master of Science in Engineering

Doctoral Advisory Committee Chair: Dr. Dmitri Vainchtein

Creating chaotic advection is the most efficient strategy to achieve mixing in a microscale or in a very viscous fluid, and it has many important applications in microfluidic devices, material processing and so on. In this paper, we present a quantitative long-term theory of resonant mixing in 3-D near-integrable flows. We use the flow in the annulus between two coaxial elliptic counter-rotating cylinders as a demonstrative model. We illustrate that such resonance phenomena as resonance and separatrix crossings accelerate mixing by causing the jumps of adiabatic invariants. We calculate the width of the mixing domain and estimate a characteristic time of mixing. We show that the resulting mixing can be described in terms of a single diffusion-type equation with a diffusion coefficient depending on the averaged effect of multiple passages through resonances. We discuss what must be done to accommodate the effects of the boundaries of the chaotic domain.

TABLE OF CONTENTS

ABSTRACT	ii
LIST OF FIGURES	v
1. INTRODUCTION	1
1.1 Chaos	2
1.2 Mixing	3
2. LITERATURE REVIEW	5
2.1 Chaotic advection	5
2.2 Averaging method and adiabatic invariant	6
2.3 Resonance phenomena and mixing	7
2.4 Applications of mixing	8
3. SETTINGS AND MAIN EQUATIONS OF THE FLOW	9
3.1 Unperturbed flow	9
3.2 The flow with perturbation	11
3.2.1 Structure of the resonance	12
3.2.2 Averaging method	13
3.2.3 Resonance variables	15
3.2.4 Scattering on resonance	16
3.2.5 Long-term chaotic advection	22

4. PROPERTY OF DIFFUSION	25
4.1 Numerical results of adiabatic spreading	25
4.2 The structure of second layer boundaries	32
5. CONCLUSIONS	34
REFERENCES	35
BIBLIOGRAPHY	38

LIST OF FIGURES

3.1	Model of Stokes Taylor-Couette.	9
3.2	Flow domain of the system in (ρ, z) plane.	12
3.3	The motion of the particle in (a) regular and (b) chaotic domain. . .	14
3.4	The motion of the particle plotted in (ρ, z) plane.	14
3.5	Schematic phase portraits on the $(\theta, \dot{\theta})$	15
3.6	The plot of $\Delta\rho(\xi)/\sqrt{\varepsilon}$ as function of ξ	18
3.7	The motion of particles between first and second layer boundaries plotted in (ρ, z) plane.	19
3.8	The plot of $\Delta\rho$ as function of θ for different values of ρ	20
3.9	The variance of distribution of $\Delta\rho$ as function of ρ	21
3.10	Comparison of improved AI with original AI(ρ).	22
3.11	The diffusion coefficient, $D(\rho)$, as function of ρ	23
4.1	The histogram of $\Psi(\rho, N)$ after different numbers of resonance crossings for box1.	26
4.2	The histogram of $\Psi(\rho - \langle\rho_0\rangle, N)$ after different numbers of resonance crossings for box1.	27
4.3	The variance of ρ , over 1000 trajectories as a function of the number of resonance crossings for box1.	27
4.4	The mean value of ρ over 1000 trajectories as a function of the number of resonance crossings for box1.	27

4.5	The histogram of $\Psi(\rho, N)$ after different numbers of resonance crossings for box2.	28
4.6	The histogram of $\Psi(\rho - \langle \rho_0 \rangle, N)$ after different numbers of resonance crossings for box2.	28
4.7	The variance of ρ , over 1000 trajectories as a function of the number of resonance crossings for box2.	28
4.8	The mean value of ρ over 1000 trajectories as a function of the number of resonance crossings for box2.	29
4.9	The histogram of $\Psi(\rho, N)$ after different numbers of resonance crossings for box3.	29
4.10	The histogram of $\Psi(\rho - \langle \rho_0 \rangle, N)$ after different numbers of resonance crossings for box3.	29
4.11	The variance of ρ , over 1000 trajectories as a function of the number of resonance crossings for box3.	30
4.12	The mean value of ρ over 1000 trajectories as a function of the number of resonance crossings for box3.	30
4.13	The histogram of $\Psi(\rho, N)$ after different numbers of resonance crossings for box4.	30
4.14	The histogram of $\Psi(\rho - \langle \rho_0 \rangle, N)$ after different numbers of resonance crossings for box4.	31
4.15	The variance of ρ , over 1000 trajectories as a function of the number of resonance crossings for box4.	31
4.16	The mean value of ρ over 1000 trajectories as a function of the number of resonance crossings for box4.	31
4.17	The plot of the first and second layer boundaries in (ρ, z) plane.	32
4.18	Number of particles out of chaotic boundary for $\langle \rho_0 \rangle = 2.236$	33
4.19	Number of particles out of chaotic boundary for $\langle \rho_0 \rangle = 2.335$	33

4.20	Number of particles out of chaotic boundary for $\langle \rho_0 \rangle = 2.556$	33
------	--	----

1. INTRODUCTION

Mixing problems appear in a wide range of applications. Although creating turbulent flows is a common method to achieve mixing, it works only in flows with a high Reynolds number. It is really difficult to create turbulent flow on a microscale or in very viscous fluids. In these cases the most efficient strategy to achieve mixing is to create chaotic advection (advection means that particles in the fluid always follow the streamlines, and the inertial of the particles can be neglected). There are many important applications of the chaotic advection, for example, in microfluidic devices, material processing, chemistry, heat transfer, and so on.

The mixing process is quite complicated in many systems, so the aim of this study is to construct a simple mathematic model to describe the chaotic advection caused by resonance phenomena. The main purpose here is not to construct a detailed description of our specific problem but rather to develop an approach for a broad class of problems and to generate intuition about what might happen in more complex situations. D.L.Vainchtein, A.I.Neishtadt and I.Mezic proposed a general theory of scattering on resonances and capture into resonances in volume-preserving systems. In [9], they considered a 3D flow field between two coaxial counter-rotating cylinders. They described what happens during a single passage through the resonance and showed that the accumulation of the effects of multiple passages through the resonance leads to the destruction of the adiabatic invariancy and chaotic advection. They estimated the width of the chaotic domain, and the characteristic time of mixing. They proposed that the boundaries of the chaotic domain are the streamlines tangential to the resonance surface. Streamlines between those boundaries intersect

the resonance surface, while those outside the boundaries do not. They proposed that the resultant mixing can be qualitatively described by a diffusion type equation with a diffusion coefficient depending on the average effect of multiple passages through the resonance.

Based on the results and theory developed before, we improve the analytical description of the long-term evolution of the system and it is supported with numerical simulations. In particular we prove that the long-term mixing can be quantitatively described by the diffusion type equation.

The structure of the thesis is as follows: Chapter 1 is the introduction of the general theory of scattering on resonances in volume-preserving systems and settings of the model under study. Chapter 2 is the review of current literature. Chapter 3 presents the main equations of the system under study, and main definitions and terminologies. Chapter 4 presents long-term chaotic behavior of the system and new discoveries near boundaries of the chaotic domain of the system. Chapter 5 is the conclusion of the research.

1.1 *Chaos*

Chaos theory is a topic in mathematics, physics, economics, and philosophy studying the behavior of dynamical systems that are highly sensitive to initial conditions. Chaotic behavior has been observed in a variety of systems in fluid dynamics, mechanical and magneto-mechanical devices, electrical circuits, lasers, and chemical reactions. Observations of chaotic behavior in nature include changes in weather, population growth in ecology, and so on.

Lorenz started to study the chaotic behavior of weather in 1950s and set up a simplified model [7], for which he found that the solutions never settled down to an equilibrium or to a periodic state. He also showed that slightly different initial conditions resulted in totally different behaviors. The implication was that the system

was inherently unpredictable, because the tiny errors in measuring the current state of the atmosphere would be amplified rapidly, eventually leading to embarrassing forecasts.

A few years later, many examples of chaos in iterated maps were found in population biology. Later, Feigenbaum [17] discovered that there are certain universal laws governing the transition from regular to chaotic behavior; roughly speaking, completely different systems go chaotic in the same way. Finally, many experimentalists such as Gollub and Libchaber [18] tested the new ideas about chaos in experiments on fluids, chemical reactions, electronic circuits, mechanical oscillators, and semiconductors.

The formal definition of chaos [1] is aperiodic long-term behavior in a system that exhibits sensitive dependence on initial conditions. (1) "Aperiodic long-term behavior" means that there are trajectories which do not settle down to fixed points, periodic orbits, or quasiperiodic orbits as $t \rightarrow \infty$. For practical reasons, we should require that such trajectories are not too rare. For instance, we could insist that there should be an open set of initial conditions leading to aperiodic trajectories, or perhaps that such trajectories should occur with nonzero probability, given a random initial condition. (2) "Sensitive dependence on initial conditions" means that nearby trajectories separate exponentially fast, i.e., the system has a positive Liapunov exponent. Small changes of initial conditions will make the system behave totally differently.

1.2 *Mixing*

Mixing is one of the most popular areas implementing chaos theory. As we know, viscous fluids are not easily mixed. For example, much effort is required to mix honey and sugar syrup. One of the reasons for this challenge is that turbulence is nonexistent for such viscous flows. However, in such flows, certain simple dynamics gives rise to chaotic behavior of particles' trajectories, and it helps to mix the viscous fluids more

easily. It is known as chaotic advection, which refers to the chaotic motion of particles in a laminar flow.

Creating chaotic advection in the fluid makes neighboring fluid particles separate exponentially with time, and particles spread over different regions of the fluid relatively quickly which is a requirement for efficient mixing. For instance, the chaotic advection is visualized as beautifully elongated structures stretch-and-fold in dye spreading experiments. Nowadays, many industrial processes benefit from a better understanding of mixing. This might partly explain the enthusiasm generated by chaotic advection. In the following chapter, we will discuss the chaotic advection in more detail.

2. LITERATURE REVIEW

2.1 Chaotic advection

When a particle moves with the fluid, the advection means that the particle can do nothing but follow the fluid, instantaneously adjusting its own velocity to that of the ambient flow:

$$V_{\text{particle}} = V_{\text{fluid}}. \quad (2.1)$$

The particle's velocity, V_{particle} , is given by the rate of change of its position:

$$V_{\text{particle}} = \left(\frac{dx}{dt}, \frac{dy}{dt}, \frac{dz}{dt} \right), \quad (2.2)$$

where (x, y, z) is the position vector of the particle in Cartesian coordinates. We also assume that the velocity component of the fluid is given by,

$$V_{\text{fluid}} = [u(x, y, z, t), v(x, y, z, t), w(x, y, z, t)]. \quad (2.3)$$

The condition that the particle's velocity equals fluid velocity leads to a system of ordinary differential equations(ODEs) called advection equations:

$$\begin{aligned} \frac{dx}{dt} &= u(x, y, z, t), \\ \frac{dy}{dt} &= v(x, y, z, t), \end{aligned}$$

$$\frac{dz}{dt} = w(x, y, z, t). \quad (2.4)$$

In 3D the flow need not be time-dependent in order to have chaos; steady flow will do. In 2D the flow must be time-dependent to produce chaotic particle motion. Two-dimensional kinematics of advection by an incompressible flow is equivalent to the Hamiltonian dynamics of a one-degree-of-freedom system. In an integrable Hamiltonian system, all the trajectories are regular. The KAM(Kolmogorov-Arnold-Moser) theorem [16] tells us that for sufficiently small nonintegrable perturbations of nonlinear integrable Hamiltonian systems, most of the KAM tori survive, and are gradually destroyed as the perturbation is increased.

2.2 Averaging method and adiabatic invariant

We consider the base flow is an integrable 3D flow that possesses two invariants [9], and we assume that almost all the streamlines are closed curves. We can write evolution equations (2.4) in the following forms:

$$\dot{I}_1 = 0, \quad \dot{I}_2 = 0, \quad \dot{\theta} = \omega(I_1, I_2). \quad (2.5)$$

Each curve is defined by the values of I_1 and I_2 and denoted as Γ_{I_1, I_2} . Now we add a small perturbation to the base flow, and the full system becomes:

$$\dot{I}_1 = \varepsilon v_1(I_1, I_2, \theta), \quad \dot{I}_2 = \varepsilon v_2(I_1, I_2, \theta), \quad \dot{\theta} = \omega(I_1, I_2) + \varepsilon g(I_1, I_2, \theta). \quad (2.6)$$

System (2.6) is volume-preserving if the right-hand side is divergence-free. For $0 < \varepsilon \ll 1$, flow (2.6) possesses two different time scales. The variable θ changes fast, of order of 1, while the variables I_1 and I_2 change very slowly, of order of ε . Thus, system (2.6) is called the slow-fast system. For a slow-fast system, if we want to analyze short time dynamics of the system, we analyze exact governing equations.

However, if we want to analyze the long time evolution, we can use the averaging method to average evolution equations over the fast period (fast variable θ). This method can simplify our analysis on the long time dynamics of the system by reducing the dimension of the system by 1. After averaging, system (2.6) becomes:

$$\begin{aligned} \dot{I}_1 &= \varepsilon \frac{1}{2\pi} \int_0^{2\pi} v_1 d\theta \\ \dot{I}_2 &= \varepsilon \frac{1}{2\pi} \int_0^{2\pi} v_2 d\theta. \end{aligned} \quad (2.7)$$

The original 3D volume-preserving system becomes a 2D volume-preserving system. Introduce the flux $\Phi(I_1, I_2)$ of the perturbation vector $V = (v_1, v_2, g)$ across a surface S spanning Γ_{I_1, I_2} :

$$\Phi(I_1, I_2) = \int_S (V \cdot n) dS. \quad (2.8)$$

The positive direction of n is the direction of angular velocity along the edge of S in the base flow. Because of the conservation of volume, the value of Φ is independent of the choice of a surface. System (2.7) can be expressed as a Hamiltonian system:

$$\dot{I}_1 = \varepsilon \frac{\partial \Phi}{\partial I_2}, \quad \dot{I}_2 = -\varepsilon \frac{\partial \Phi}{\partial I_1}. \quad (2.9)$$

Therefore, Φ is an adiabatic invariant of exact system (2.6). If $\dot{\theta}$ does not vanish anywhere along a streamline, $\Phi(I_1, I_2)$ would be conserved with the accuracy of order of ε over time which is of order of $1/\varepsilon$. However, this approximation is valid everywhere except for a small part of the space where $\dot{\theta} \approx 0$.

2.3 Resonance phenomena and mixing

For system (2.6) discussed in the previous section, the averaging method is not valid near the resonance given by $\omega(I_1, I_2) = 0$. The equation $\omega(I_1, I_2) = 0$ defines a

2D surface in the original 3D space [curves on the (I_1, I_2) plane], called the resonance surface, or the resonance. In the vicinity of the resonance, the change of θ is not fast compared to the changes in I_1 and I_2 , so we can not expect the averaged system to approximate the exact system adequately in the vicinity of the resonance.

As the trajectories pass through the resonance, the structure of streamlines becomes chaotic. A single passage through the resonance leads to the jump of adiabatic invariant [4], and multiple passages through the resonance lead to the destruction of adiabatic invariancy and chaotic advection. The accumulation of the effects of the resonance phenomena creates mixing.

2.4 *Applications of mixing*

Mixing by chaotic advection has numerous applications in diverse areas of fluid mechanics, especially for Stokes flows. There are several recent popular applications in the engineering science. First, application is in microfluidic devices, in particular in biofluidics, where the objective is to perform mixing within the microchannels of a chip. In this kind of fluids, the Reynold number is low, of order of 1. Chaotic advection provides an attractive engineering solution to achieve efficient stirring in this context.

Another important application is in the material processing. Chaotic advection offers a new method to develop fine-scale structures, and offers new opportunities to develop processes where structure development among material components can be better controlled, so that a variety of distinct material arrangements can be formed.

There are many other applications in different fields such as chemistry, heat transfer and so on.

3. SETTINGS AND MAIN EQUATIONS OF THE FLOW

In the rest of thesis we discuss a model developed by D.L.Vainchtein, A.I.Neishtadt and I.Mezić [9]. They set a model of Stokes Taylor-Couette flow between two infinite coaxial counter-rotating cylinders, shown in figure 3.1. The inner cylinder is a perfect circle and rotates in constant angular velocity, while the outer cylinder is elliptic and rotates in the opposite direction with the angular velocity periodically changing in the vertical direction.

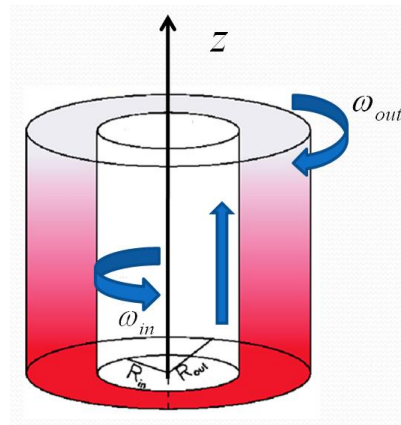


Fig. 3.1: Model of Stokes Taylor-Couette.

3.1 Unperturbed flow

The base flow is a Stokes Taylor-Couette flow between two infinite counter-rotating circular coaxial cylinders. The z_d variable is along the axes of the cylinders, r is the distance from the common axis and θ is an angle in the horizontal plane. The velocity

field is shown in following form:

$$\dot{r} = 0, \quad \dot{z}_d = 0, \quad \dot{\theta} = \omega_d(r, z_d), \quad (3.1)$$

with

$$\omega_d(r, z_d) = \omega_i \frac{r}{r_i} \left[1 - \frac{1}{1-\eta^2} (1 - \eta \frac{\omega_o}{\omega_i}) \right] + \omega_i \frac{r_i}{r} (1 - \eta \frac{\omega_o}{\omega_i}) \frac{1}{1-\eta^2}. \quad (3.2)$$

Here r_i, r_o are the radii of the inner and outer cylinders, respectively, and $\eta = r_i/r_o$.

The inner cylinder rotates with constant angular velocity ω_i , while angular velocity of the outer cylinder ω_o is given by $\omega_o = \omega_i(-1 + \delta \sin(\lambda_d z_d))$, where λ_d is the wave number and δ is the amplitude of oscillations. Thus ω_o changes periodically with z_d . Qualitatively similar results can be obtained if instead of the varying ω_o , the outer cylinder has a varying radius. Similarly, we could consider a flow inside a torus-shaped container instead of the annulus.

We change all the variables into dimensionless variables. We rescale the time by ω_i and the distances by r_i :

$$\bar{t} = t\omega_i, \quad \omega = \frac{\omega_d}{\omega_i}, \quad \rho = \frac{r}{r_i}, \quad z = \frac{z_d}{r_i}, \quad \lambda = \lambda_d r_i. \quad (3.3)$$

From now on all the variables are in the dimensionless forms and the dot denotes the derivative with respect to \bar{t} . The following set of parameters was used in our numerical results presented in the following sections:

$$r_i = 0.2, \quad r_o = 1.0, \quad \eta = 0.2, \quad \delta = 0.4, \quad \lambda = 2\pi. \quad (3.4)$$

The value of ρ changes between $\rho = 1$ (at the inner cylinder) and $\rho = (1/\eta) = 5$

(at the outer cylinder). For $\omega(\rho, z)$, we have:

$$\omega(\rho, z) = -\rho \frac{\eta}{1-\eta} + \frac{1}{\rho} \frac{1}{1-\eta} + \frac{\eta}{1-\eta^2} \delta \sin(\lambda z) \left(\rho - \frac{1}{\rho}\right). \quad (3.5)$$

In unperturbed system (3.1), everything moves nice and smooth. The trajectories in (ρ, z) plane are straight lines with constant values of ρ .

3.2 The flow with perturbation

A perturbation consists of two parts. The first is a vertical (in the axial direction) shear-type flow. We slowly pull up the inner cylinder in z direction with velocity in order of ε , and $0 < \varepsilon \ll 1$ is a small parameter. The second is the cross section of the outer cylinder is not a perfect cycle. It is elliptic, and its major axis a and minor axis b have the following relationship:

$$\frac{a}{b} - 1 = \varepsilon \kappa. \quad (3.6)$$

Parameter $\kappa \sim 1$ defines a characteristic ratio of the two perturbations. The full 3D flow is given by

$$\begin{aligned} \dot{\rho} &= \varepsilon \kappa (\rho - 1) \cos \theta, \\ \dot{z} &= \varepsilon (1 + \ln \rho / \ln \eta), \\ \dot{\theta} &= \omega(\rho, z) - \frac{1}{\rho} \varepsilon \kappa (2\rho - 1) \sin \theta. \end{aligned} \quad (3.7)$$

System (3.7) is a volume-preserving system. The axial velocity \dot{z} equals ε at $\rho = 1$ and vanishes at $\rho = 1/\eta$. In a limiting case of $\kappa = 0$, when the outer cylinder is circular, the flow possesses the axial symmetry. Note that the reason for choosing both perturbations to be of the same order is that it is the interaction between the two perturbations that results in chaotic advection.

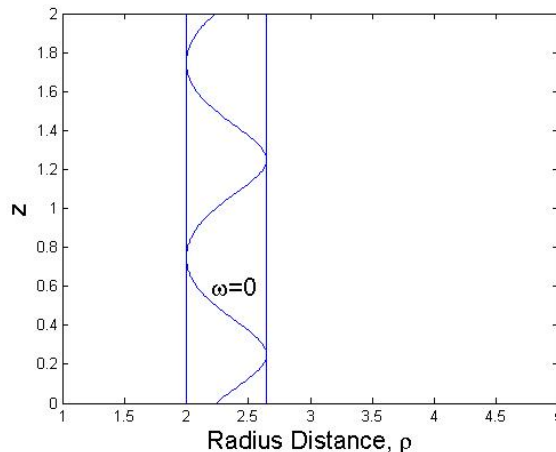


Fig. 3.2: Flow domain of the system in (ρ, z) plane.

The right-hand side of (3.7) depends on z periodically with a period $2\pi/\lambda$ (1 for $\lambda = 2\pi$) while z itself changes monotonically, regardless of the values of other variables. Therefore, in all the figures below, we assume periodic boundary conditions in z with a period 1.

3.2.1 Structure of the resonance

The wavy line in the middle of figure 3.2 is the resonance given by $\omega(\rho, z) = 0$, and the vertical lines are tangential to the resonance surface. Trajectories between two vertical lines intersect with the resonance, while those outside vertical lines do not. The width of the domain between two vertical lines is calculated using (3.5) in condition $\omega = 0$. The resonance surface R is given as a function of z in the following form:

$$\rho_R(z) = \sqrt{\frac{1 + \eta - \eta\delta \sin(\lambda z)}{\eta + \eta - \delta \sin(\lambda z)}}. \quad (3.8)$$

Depending on equation (3.8), the minimum and maximum values of $\rho_R(z)$, respec-

tively, are given by

$$\rho_{\min} = \sqrt{\frac{1 + \eta + \eta\delta}{\eta(1 + \eta + \delta)}}, \quad \text{and} \quad \rho_{\max} = \sqrt{\frac{1 + \eta - \eta\delta}{\eta(1 + \eta - \delta)}}. \quad (3.9)$$

Depending on values of the parameters defined in (3.4), we can calculate the width of the mixing domain which is located between

$$\rho_{\min} = 2 \quad \text{and} \quad \rho_{\max} = \sqrt{7} \approx 2.6458. \quad (3.10)$$

The domain between ρ_{\min} and ρ_{\max} is known as the chaotic domain, and the domain outside ρ_{\min} and ρ_{\max} is known as the regular domain.

3.2.2 Averaging method

Far from the resonance, which was defined in the previous section, the variables ρ and z change slowly, $\propto \varepsilon$ and the variable θ changes relatively fast, $\dot{\theta} \sim 1$. Thus, we can use the averaging method to average the evolution equations over the fast variable θ to get the averaged equations of motion:

$$\dot{\rho} = 0, \quad \dot{z} = \varepsilon(1 + \ln\rho/\ln\eta). \quad (3.11)$$

The averaged trajectories [in the full 3D, (ρ, z, θ) , space] spiral around the cylinders of constant radius with the direction of the rotation depending on the sign of ω . System (3.11) can be written as Hamiltonian equations, and ρ is an invariant. It is also an adiabatic invariant of the exact system. In the absence of the resonance, it would stay within order ε from the initial value over time of order $1/\varepsilon$, which is shown in figure 3.3a. The trajectories in the regular domain plotted in (ρ, z) plane are just straight lines with constant ρ , shown in figure 3.4a.

However, when trajectories are close to the resonance, $|\dot{\theta}|$ is decreasing. In the vicinity of the resonance, θ , ρ , and z change in the same order, of order of ε . Thus,

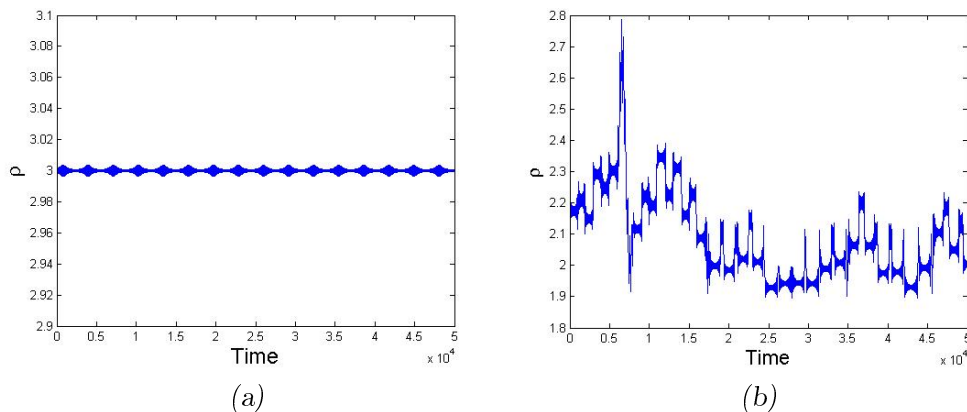


Fig. 3.3: The motion of the particle in (a) regular and (b) chaotic domain.

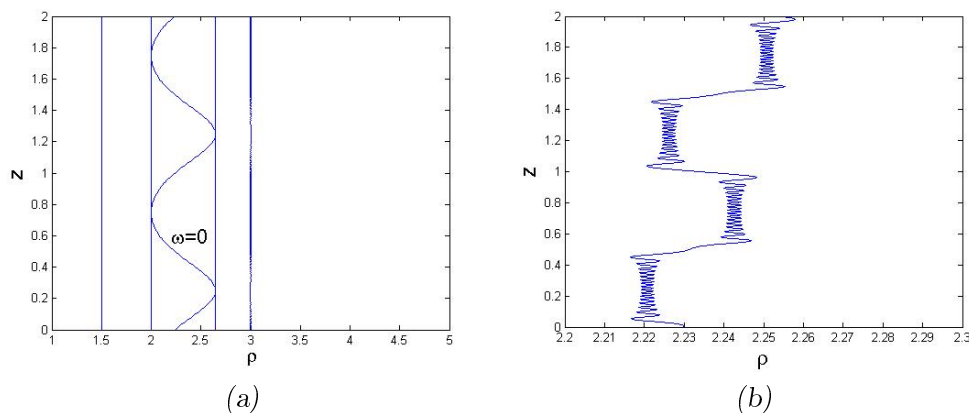


Fig. 3.4: The motion of the particle in (a) regular and (b) chaotic domain plotted in (ρ, z) plane.

the averaging method is not valid anymore. When trajectories pass through the resonance, the adiabatic invariancy breaks down. For instance, the trajectory in chaotic domain keeps constant ρ for some time, and at certain point it jumps to another value of ρ . This behavior continues all the time, and the jumps look quite random, shown in figure 3.3b. The jumps of adiabatic invariant happen when the trajectory passes through the resonance, shown in figure 3.4b. Therefore, we have to analyze the dynamics of particles separately when they are in the vicinity of the resonance.

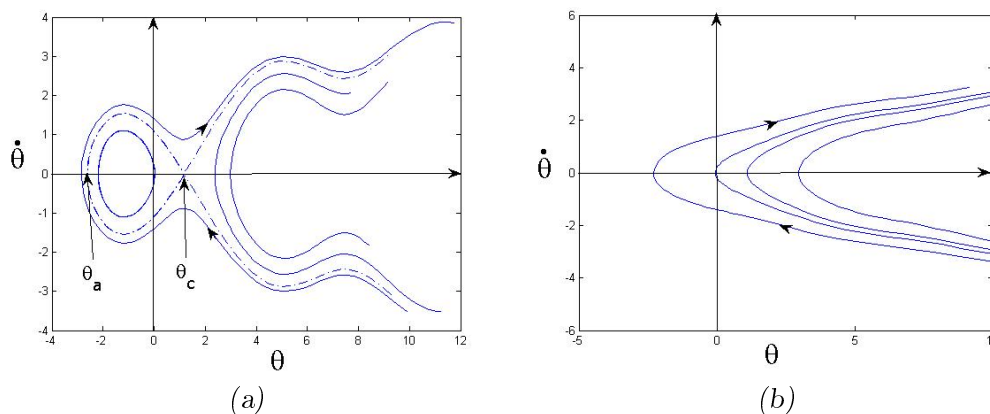


Fig. 3.5: Schematic phase portraits on the $(\theta, \dot{\theta})$ for (a) $|b_1| > |a|$ and (b) $|b_1| < |a|$.

3.2.3 Resonance variables

The equations of motion in the vicinity of the resonance are derived using changing of variables discussed in [9]:

$$\begin{aligned}\dot{\omega} &= \varepsilon f_1(\omega, \sigma, \theta), \\ \dot{\sigma} &= \varepsilon f_2(\omega, \sigma, \theta), \\ \dot{\theta} &= \omega + \varepsilon g(\omega, \sigma, \theta).\end{aligned}\tag{3.12}$$

The new variable σ is defined as,

$$\sigma = -\frac{1-\eta}{2\eta} \int_0^z \frac{\rho_R(z)}{1 - [\delta/(1+\eta)] \sin(\lambda z)} dz.\tag{3.13}$$

Note that σ is just an auxiliary variable. All the final results will be given in terms of the original variable ρ , and z , and $\rho_R(z)$ denotes the value of ρ at the resonance for the given value of z . As σ is a function of z only, we can simplify the right-hand side of equation (3.12) to the following forms:

$$f_{1,0} = a + b_1 \cos \theta,$$

$$\begin{aligned}
a &= \frac{\eta}{1-\eta^2} \delta \lambda \cos(\lambda z) \left(\rho - \frac{1}{\rho}\right) (1 + \ln \rho / \ln \eta), \\
b_1 &= -2k \frac{1}{\rho + 1},
\end{aligned} \tag{3.14}$$

and

$$f_{2,0} = -\frac{1}{2} \rho (\rho^2 - 1) (1 + \ln \rho / \ln \eta). \tag{3.15}$$

Note that $f_{1,0}$ and $f_{2,0}$ are derived from plugging the resonance condition ($\omega = 0$) into functions f_1 and f_2 . The relation between a and b_1 defines the properties of the phase portrait on the (θ, θ') phase plane. If

$$|b_1| > |a|, \tag{3.16}$$

the phase portrait looks like the one shown in figure 3.5a. If (3.16) does not hold, the phase portrait looks like the one shown in figure 3.5b. Notice that these figures correspond to $a > 0$. For $a < 0$ the plots should be reflected with respect to the vertical axis and the direction of the arrows reversed. Note that $a = 0$ at $\lambda z = \pi/2$ and $\lambda z = 3\pi/2$ (where $\cos(\lambda z) = 0$). Therefore, while in the center of the mixing region condition (3.16) may be satisfied or not, there are always zones near the edges of the mixing regions where (3.16) is satisfied.

3.2.4 Scattering on resonance

Jump of AI between first layer boundaries

We name the two vertical lines tangential to the resonance surface the *first layer boundaries* of the chaotic domain shown in figure 3.2. The position of inner and outer first layer boundaries is at $\rho_{\text{inner}} = 2$, and $\rho_{\text{outer}} = 2.6458$ from (3.10). The single jump of adiabatic invariant $\Delta\rho$ between first layer boundaries can be calculated using

the following expression:

$$\Delta\rho = -2s\sqrt{\varepsilon}\kappa(\rho - 1) \int_{s\infty}^{\bar{\theta}_*} \frac{\cos\theta}{\sqrt{2(h_* - V)}} d\theta, \quad (3.17)$$

where $s = \text{sign}(a)$. H_R is the resonance energy given by

$$H_R = \frac{1}{2}(\dot{\theta})^2 + V. \quad (3.18)$$

The resonance potential, V , is

$$V(\rho, \theta) = -a\theta - b_1 \sin\theta - V_c, \quad (3.19)$$

where V_c is the value of V at the hyperbolic fixed point θ_c in figure 3.5a,

$$V_c = -a\theta_c - b_1 \sin\theta_c; \quad \cos\theta_c = -a/b_1. \quad (3.20)$$

The value of ρ must be taken at the moment of crossing, and θ_* and h_* are the values of θ and H_R , respectively, when the exact trajectory is at resonance R . The potential $V = 0$ at special points θ_c and θ_a at the resonance. In terms of ξ , we can write (3.17) as

$$\Delta\rho = -2s\sqrt{\varepsilon}\kappa \frac{\rho - 1}{\sqrt{|a|}} \int_{s\infty}^{\bar{\theta}_*} \frac{\cos\theta}{\sqrt{2|s2\pi\xi + \theta + (b_1/a)\sin\theta|}} d\theta, \quad (3.21)$$

with

$$\xi = \text{Fractional part}\left\{\frac{h_*}{2\pi|a|}\right\}.$$

Note that ξ is a variable uniformly distributed on $(0,1)$ and it is very sensitive to the initial condition. A change of order of ε in the initial condition results in an

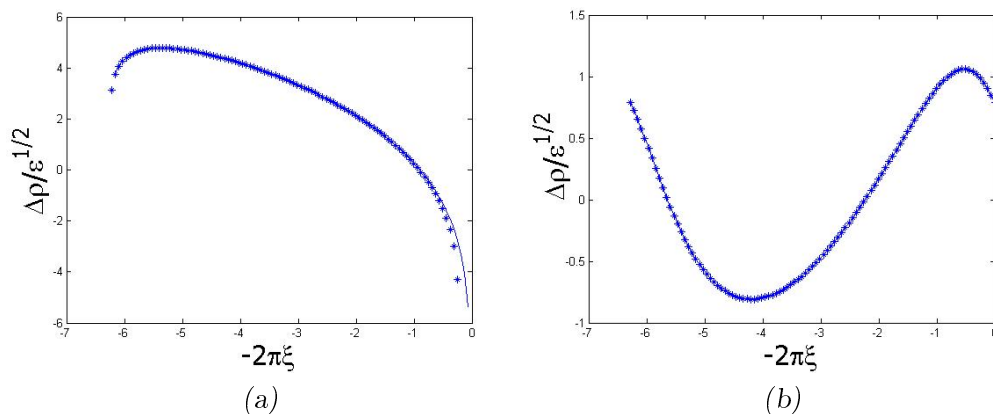


Fig. 3.6: The plot of $\Delta\rho(\xi)/\sqrt{\varepsilon}$ as function of ξ for (a) $\kappa = 2$ and (b) $\kappa = 0.2$.

order 1 change in ξ . For multiple resonance crossings, ξ can be treated as a random variable. Statistical properties of the scattering depend on the shape of the phase portrait on the $(\theta, \dot{\theta})$ plane. If the phase portrait look like the one shown in figure 3.5a, the ensemble average of $\Delta\rho$ is

$$\langle \Delta\rho \rangle = -s\sqrt{\varepsilon} \frac{\rho^2 - 1}{2\pi} S_R, \quad (3.22)$$

where S_R is the area under the separatrix loop in figure 3.5a,

$$S_R = 2 \left| \int_{\theta_a}^{\theta_c} \sqrt{-2V} d\theta \right|. \quad (3.23)$$

If the phase portrait look like the one shown in figure 3.5b, $\langle \Delta\rho \rangle = 0$, as there is no separatrix, $S_R = 0$.

We calculated $\Delta\rho(\xi)/\sqrt{\varepsilon}$ for various values of parameter ξ using equation(3.21), and compared it with the results of numerical simulations obtained by direct integration of (3.7). In figures 3.6a and 3.6b, the plots represent $\Delta\rho(\xi)/\sqrt{\varepsilon}$ as a function of ξ , respectively, for $\kappa = 2$ and $\kappa = 0.2$. The solid lines correspond to analytical values calculated from equation(3.21), and asterisks correspond to the values obtained

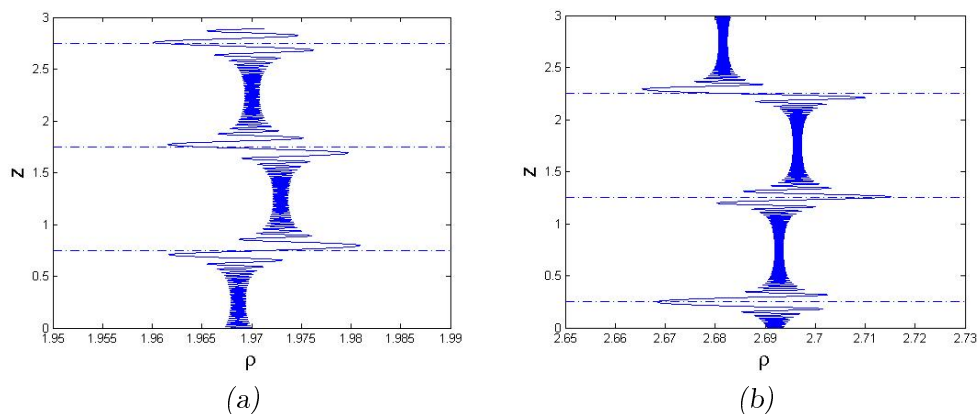


Fig. 3.7: The motion of particles between (a) inner and (b) outer side of first and second layer boundaries plotted in (ρ, z) plane.

numerically from equation(3.7). In figure 3.6a, $\kappa = 2$ and $|b_1| > |a|$, the $\Delta\rho(\xi)$ has a singularity. Therefore, there is a small possibility of large changes in ρ in the process of scattering. However, as this singularity is logarithmic, $\langle\Delta\rho\rangle$ is finite. The values of ρ in the right-hand side of equations(3.21) and (3.22) are, strictly speaking, those at the moment of crossings. But, as characteristic values of $\Delta\rho$ of a single crossing are small, if we specify the initial conditions far from the resonance, we can use those values of ρ in equations(3.21) and (3.22).

One can see that $\langle\Delta\rho\rangle > 0$ if $\cos(\lambda z) < 0$ and $\langle\Delta\rho\rangle < 0$ if $\cos(\lambda z) > 0$. As a single jump is small, two consecutive crossings occur at almost the same values of ρ and S_R . Therefore, it follows from equation(3.22) that the average change in ρ during one z period is zero.

Jump of AI between first and second layer boundaries

The numerical results in following sections show that there is large transport of particles between the domain inside first layer boundaries and the domain outside first layer boundaries. We find out that the jump of the adiabatic invariant also happens for particles in the domain outside first layer boundaries, where the resonance does

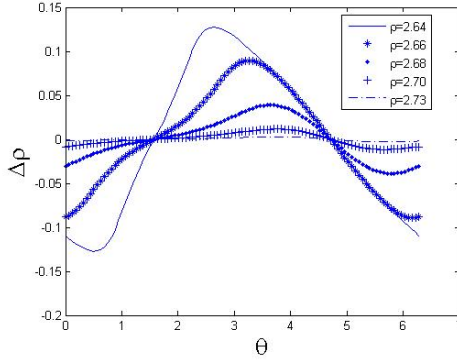


Fig. 3.8: The plot of $\Delta\rho$ as function of θ for different values of ρ .

not exist. The jump of adiabatic invariant happens at $z_1 = 3/4$ ($\sin(\lambda z_1) = -1$), near the inner first layer boundary, shown in figure 3.7a. The jump of adiabatic invariant happens at $z_0 = 1/4$ ($\sin(\lambda z_0) = 1$), near the outer first layer boundary, shown in figure 3.7b. The jump of adiabatic invariant happens once in each slow period in the domain outside first layer boundaries, instead of twice in each slow period in the domain between first layer boundaries.

The magnitude of $\Delta\rho$ outside first layer boundaries depends on both θ and the distance between the particle and the first layer boundary, shown in figure 3.8. When particles are close to the first layer boundaries, the magnitude of $\Delta\rho$ is large, and ω is relative small (of order of $\sqrt{\varepsilon}$) at z_1 close to the inner first layer boundary, and at z_0 close to the outer first layer boundary. As particles moving further from the first layer boundaries, ω increases and the magnitude of $\Delta\rho$ decreases. Figure 3.9 represents the variance of the distribution of $\Delta\rho$ for uniformly distributed θ as the function of ρ . The absolute values of $\Delta\rho$ and the variance of the distribution of $\Delta\rho$ decrease as the distance between particles and the first layer boundaries increases. We can use the variance of $\Delta\rho$ to estimate the approximate position of the boundaries which the streamlines that start in the mixing domain do not penetrate. The boundaries are named second layer boundaries or last invariant tori, and they are the actual

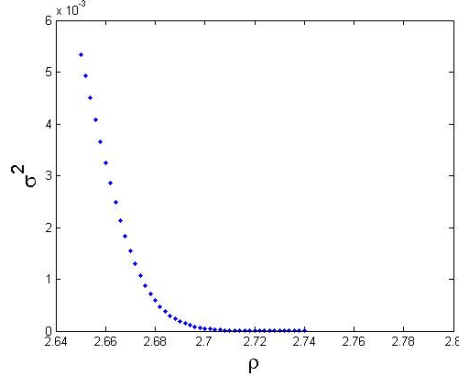


Fig. 3.9: The variance of distribution of $\Delta\rho$ as function of ρ .

boundaries of the chaotic domain.

Improved AI

As discussed in the previous section, when particles are in the region between first and second layer boundaries, as the distance between particles and the first layer boundaries increases, the magnitude of jumps of adiabatic invariant decreases. If this distance keep increasing, it becomes really difficult to distinguish the jumps of adiabatic invariant from oscillations of adiabatic invariant. In this situation the improved adiabatic invariant is very useful. The improved adiabatic invariant $\bar{\rho}$ is given by,

$$\bar{\rho} = \rho - \varepsilon\kappa \frac{\rho - 1}{\omega} \sin \theta. \quad (3.24)$$

The change of $\bar{\rho}$ is of order of ε^2 , shown in equation(3.25). Improved adiabatic invariant $\bar{\rho}$ has a singularity at the resonance. This property of $\bar{\rho}$ helps to distinguish $\Delta\bar{\rho}$ from oscillations of $\bar{\rho}$, shown in figure 3.10.

$$\frac{d\bar{\rho}}{dt} = \varepsilon\kappa \frac{\sin \theta}{\omega} \left[\frac{\rho - 1}{\omega} \left(\frac{\partial \omega}{\partial \rho} \dot{\rho} + \frac{\partial \omega}{\partial z} \dot{z} \right) - \dot{\rho} \right] \quad (3.25)$$

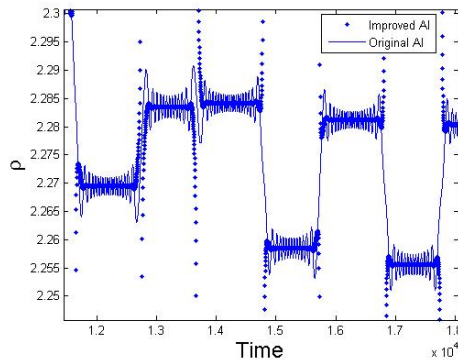


Fig. 3.10: Comparison of improved AI with original AI(ρ).

3.2.5 Long-term chaotic advection

The accumulation of the effects of the jumps of adiabatic invariant leads to the destruction of adiabatic invariance and the chaotic advection in 3D volume-preserving flows. There are two quantities that describe the chaotic advection: the size of the chaotic domain and a characteristic rate of mixing inside the chaotic domain.

The chaotic domain is separated into three parts, represented as A , B_i , B_o . Domain A is between the first layer boundaries, B_i is the domain between the inner first layer and inner second layer boundaries, and B_o is the domain between the outer first layer and outer second layer boundaries. The size and the location of A depend on the size of the annulus, η , and the amplitude of the frequency oscillation, δ , and is independent of ε . However, the sizes of B_i and B_o not only depend on η and δ , but depend on ε as well. As ε decreases, domain B_i and B_o squeeze. When ε goes to zero, the sizes of B_i and B_o go to zero, and the second layer boundaries overlap with the first layer boundaries. For instance, the second layer boundaries are much closer to the first layer boundaries for $\varepsilon = 10^{-4}$ than they are for $\varepsilon = 10^{-3}$.

We can estimate the rate of mixing by assuming the statistical independence of consecutive crossings. Recall that for multiple resonance crossings, ξ can be viewed as a random variable, and the jump of adiabatic invariant can be treated as a random walk with a characteristic step of order of $\sqrt{\varepsilon}$. Hence, after N resonance crossings,

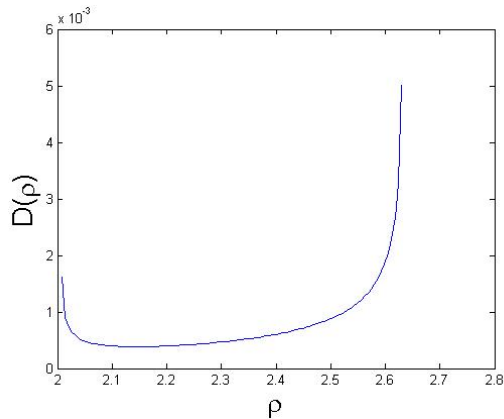


Fig. 3.11: The diffusion coefficient, $D(\rho)$, as function of ρ .

a value of ρ changes by a quantity of order of $\sqrt{N} \times \sqrt{\varepsilon}$. The mixing can be called complete if a trajectory spreads all over a chaotic domain, and the difference of ρ between inner and outer chaotic boundaries is of order of 1. Thus, it takes $N \sim 1/\varepsilon$ resonance crossings to complete the diffusion. The time between two successive resonance crossings is of order of $1/\varepsilon$, so the characteristic time of mixing T_M is of order of ε^{-2} . For $\varepsilon = 0$, the rate of mixing $1/T_M$ vanishes, and the dynamics is regular. As $\varepsilon \rightarrow 0$, it takes a longer and longer time for streamlines to mix, $T_M \rightarrow \infty$.

Many systems with random walks are described using diffusion equations, that for the system under consideration can be written as

$$\frac{\partial \Psi_D}{\partial N} = \frac{\partial}{\partial \rho} \left(D(\rho) \frac{\partial \Psi_D}{\partial \rho} \right). \quad (3.26)$$

In (3.26) Ψ_D is a probability distribution function, which denotes the number of trajectories having the value of ρ in the interval $\rho \pm \varepsilon$ after N resonance crossings. The diffusion coefficient, $D(\rho)$ is given by the dispersion of $\Delta\rho_\Sigma$.

$$D(\rho) = \int_0^1 (\Delta\rho(\xi) - \langle \Delta\rho \rangle)^2 d\xi. \quad (3.27)$$

The profile of $D(\rho)$ as a function of ρ for $\kappa = 0.2$ is presented in figure 3.11. The values of other parameters are specified in (3.4).

The boundary conditions used for solving diffusion equation (3.26) are

$$\begin{aligned}\frac{\partial \Psi}{\partial \rho} \Big|_{\rho=2.0085} &= 0, \\ \frac{\partial \Psi}{\partial \rho} \Big|_{\rho=2.6301} &= 0.\end{aligned}\tag{3.28}$$

This boundary conditions are given by condition $|b_1| < |a|$, to make sure all particles are pure scattering.

4. PROPERTY OF DIFFUSION

4.1 Numerical results of adiabatic spreading

In [9], Vainchtein, Neishtadt, and Mezić proposed that the mixing process can be qualitatively described by the diffusion type equation (3.26), but they did not quantitatively demonstrate it. To quantitatively check the validity of the theory developed in [9], we performed a set of numerical simulations using the values of parameters specified in (3.4) and $\varepsilon = 10^{-3}$, $\kappa = 0.2$. We took 1000 different particles uniformly distributed in a small cubic box in the size of ε . We took 4 boxes (box1, box2, box3 and box4) from different positions in the chaotic domain. Box1, box2 and box3 were picked from the middle of the chaotic domain, and respectively the size of box1 was $\rho_{\text{in}} \times z_{\text{in}} \times \theta_{\text{in}} = [2.220, 2.229] \times [0.251, 0.260] \times [0.011, 0, 0.020]$, the size of box2 was $\rho_{\text{in}} \times z_{\text{in}} \times \theta_{\text{in}} = [2.232, 2.241] \times [0.251, 0.260] \times [1.100, 1.109]$, and the size of box3 was $\rho_{\text{in}} \times z_{\text{in}} \times \theta_{\text{in}} = [2.331, 2.34] \times [0.251, 0.260] \times [0.001, 0.01]$. We picked box4 close to the outer first layer boundary with the size of $\rho_{\text{in}} \times z_{\text{in}} \times \theta_{\text{in}} = [2.551, 2.560] \times [0.251, 0.260] \times [0.001, 0.010]$. We considered the Poincaré sections located at $z = N + 0.25$ and $z = N + 0.75$, where N is a set of integer numbers. Every trajectory crosses the resonance once between two consecutive sections.

The results of our numerical simulations for 4 different boxes showed that the particles which initially concentrated in those small boxes start to diffuse after multiple resonance crossings, and in the end, the distribution of particles in the radius direction is quite uniform, shown in figure 4.1 for box1. The solid line in figure 4.1 is

the solution of the diffusion equation (3.26) using box1 as the initial condition, and both results are consistent with each other. The same results are also obtained for other boxes.

The second moment of the distribution function $\Psi(\rho, N)$ of numerical simulations for box1, σ^2 , is shown as the dash line in figure 4.3. The constant slope of the solid line in figure 4.3 is the diffusion coefficient $D(\rho)$ analytically calculated using equation (3.27) for box1 ($\langle \rho_0 \rangle = 2.225$). The second moment of numerical simulations σ^2 is very close to $D(\rho)$ in the beginning, before particles reaching the first layer boundaries. However, when particles start to cross the first layer boundaries, σ^2 and $D(\rho)$ start to diverge. In the end, σ^2 comes to an asymptotic value with small oscillations. That asymptotic value is the variance of uniformly distributed particles in the chaotic domain, shown as horizontal lines in figure 4.3. The same results are also obtained for box2 ($\langle \rho_0 \rangle = 2.236$) and box3 ($\langle \rho_0 \rangle = 2.335$). However, the second moment of the distribution function $\Psi(\rho, N)$ for box4 ($\langle \rho_0 \rangle = 2.556$) does not follow $D(\rho)$ at all, and it means the diffusion coefficient(3.27) need to be modified near the boundaries of the chaotic domain in order to match the numerical simulations.

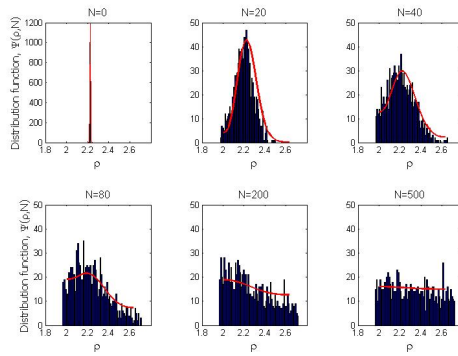


Fig. 4.1: The histogram of $\Psi(\rho, N)$ after different numbers of resonance crossings for box1.

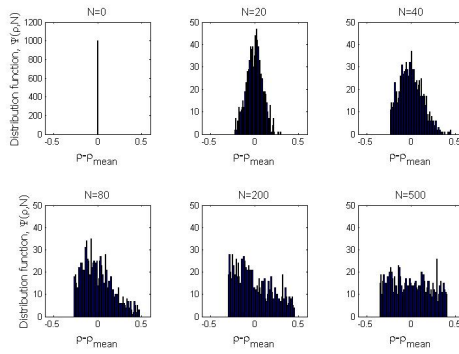


Fig. 4.2: The histogram of $\Psi(\rho - \langle \rho_0 \rangle, N)$ after different numbers of resonance crossings for box1.

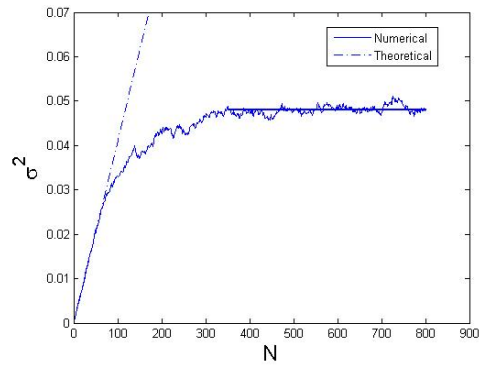


Fig. 4.3: The variance of ρ , over 1000 trajectories as a function of the number of resonance crossings for box1.

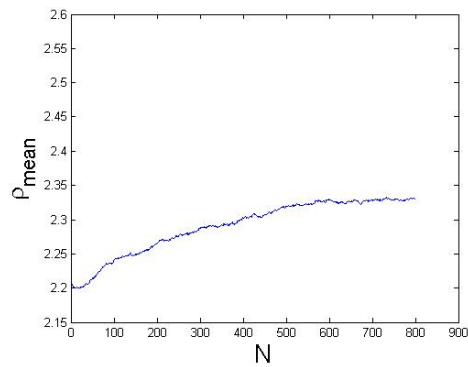


Fig. 4.4: The mean value of ρ over 1000 trajectories as a function of the number of resonance crossings for box1.

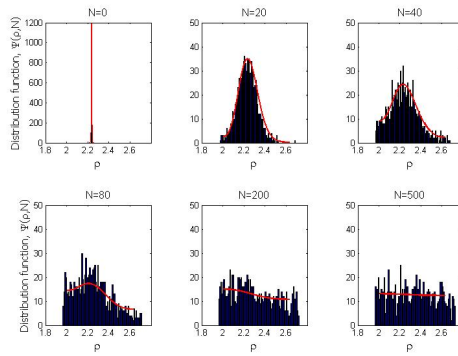


Fig. 4.5: The histogram of $\Psi(\rho, N)$ after different numbers of resonance crossings for box2.

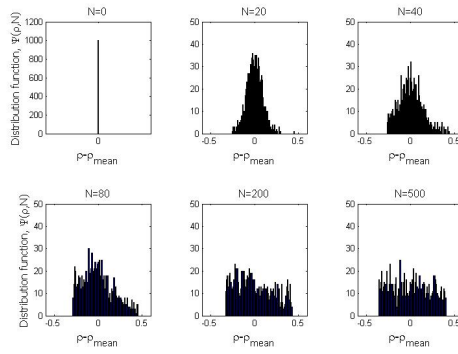


Fig. 4.6: The histogram of $\Psi(\rho - \langle \rho_0 \rangle, N)$ after different numbers of resonance crossings for box2.

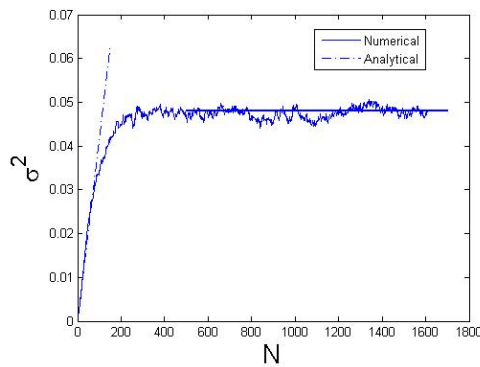


Fig. 4.7: The variance of ρ , over 1000 trajectories as a function of the number of resonance crossings for box2.

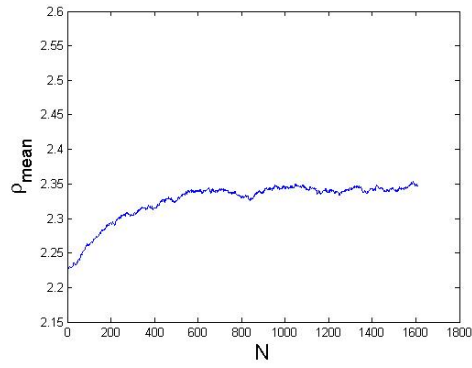


Fig. 4.8: The mean value of ρ over 1000 trajectories as a function of the number of resonance crossings for box2.

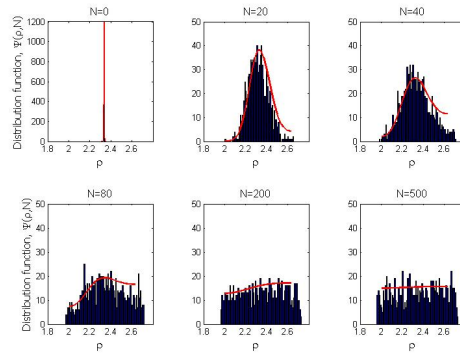


Fig. 4.9: The histogram of $\Psi(\rho, N)$ after different numbers of resonance crossings for box3.

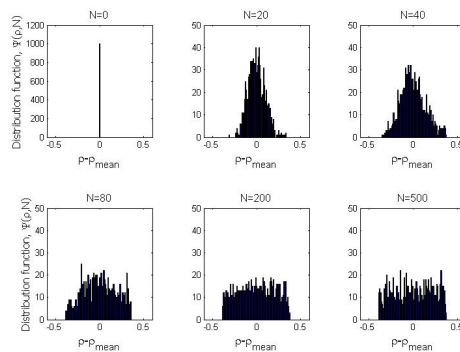


Fig. 4.10: The histogram of $\Psi(\rho - \langle \rho_0 \rangle, N)$ after different numbers of resonance crossings for box3.

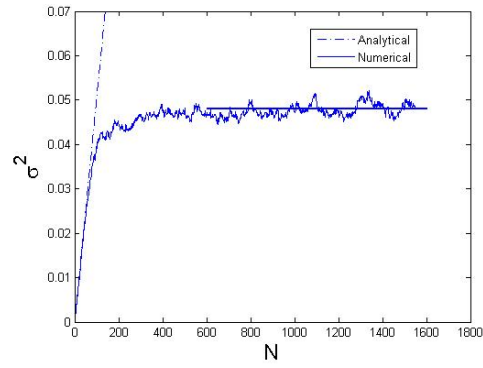


Fig. 4.11: The variance of ρ , over 1000 trajectories as a function of the number of resonance crossings for box3.

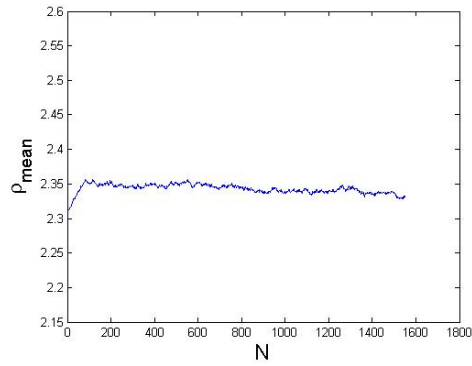


Fig. 4.12: The mean value of ρ over 1000 trajectories as a function of the number of resonance crossings for box3.

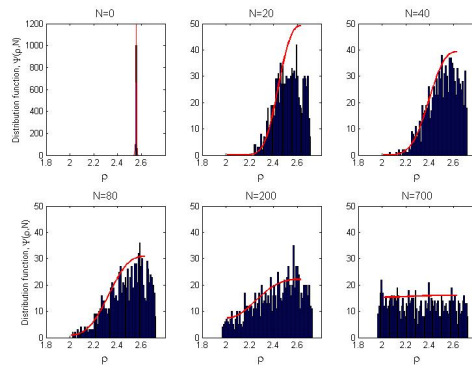


Fig. 4.13: The histogram of $\Psi(\rho, N)$ after different numbers of resonance crossings for box4.

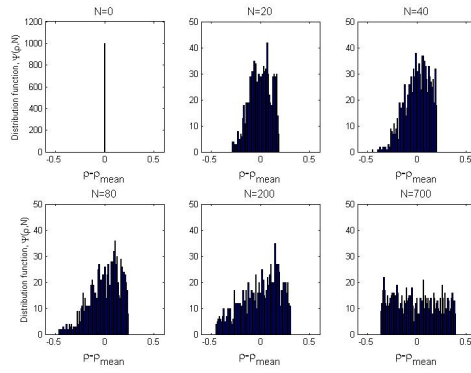


Fig. 4.14: The histogram of $\Psi(\rho - \langle \rho_0 \rangle, N)$ after different numbers of resonance crossings for box4.

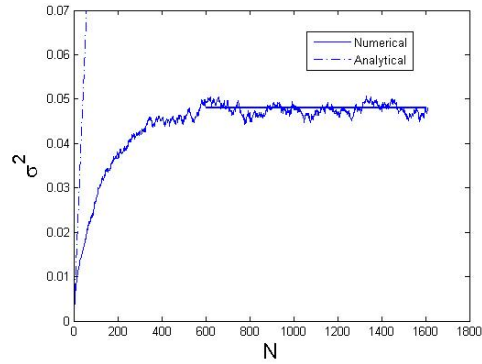


Fig. 4.15: The variance of ρ , over 1000 trajectories as a function of the number of resonance crossings for box4.

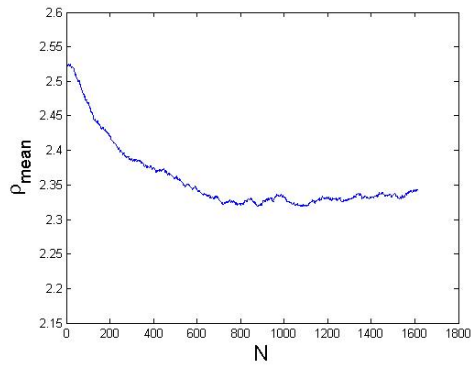


Fig. 4.16: The mean value of ρ over 1000 trajectories as a function of the number of resonance crossings for box4.

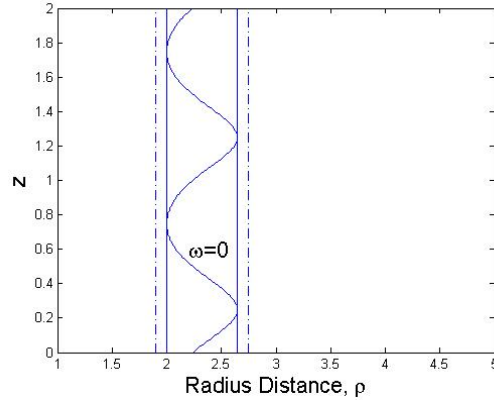


Fig. 4.17: The plot of the first and second layer boundaries in (ρ, z) plane.

4.2 The structure of second layer boundaries

The first layer boundaries is used to be thought as the boundaries of the chaotic domain. However, the results of numerical simulations showed that there is large transport of particles between the domain inside and outside first layer boundaries, shown in figure 4.5 for box2. However, those particles do not go too far from the first layer boundaries and stop at second layer boundaries, shown as the dash lines in figure 4.17. The estimated locations of second layer boundaries are at $\rho_{\text{inner}} = 1.958$ and $\rho_{\text{outer}} = 2.734$ based on the numerical results. The existence of the second layer boundaries is also proved by the second moment of distribution function $\Psi(\rho, N)$ for box2, shown in figure 4.7. The total number of particles out of first layer boundaries is approximate 1/5 of total particles when the system reaches the steady state. These results are shown in figures 4.18a and 4.18b. The same results are also obtained for box1, box3 and box4.

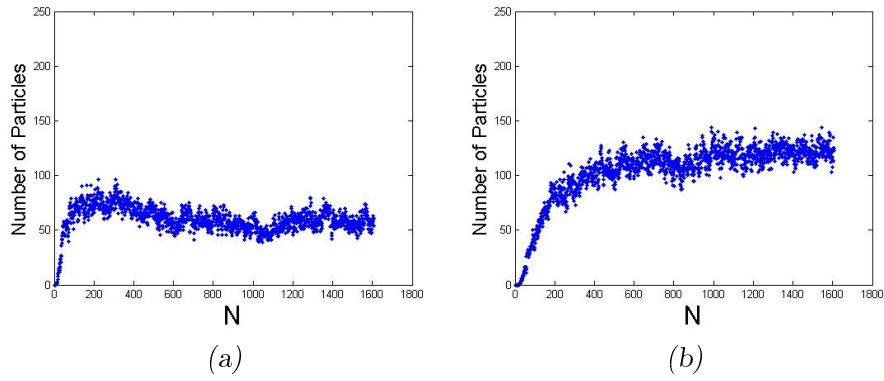


Fig. 4.18: The number of particle out of (a) inner side, and (b) outer side of the first layer boundaries versus number of resonance crossings for box2.

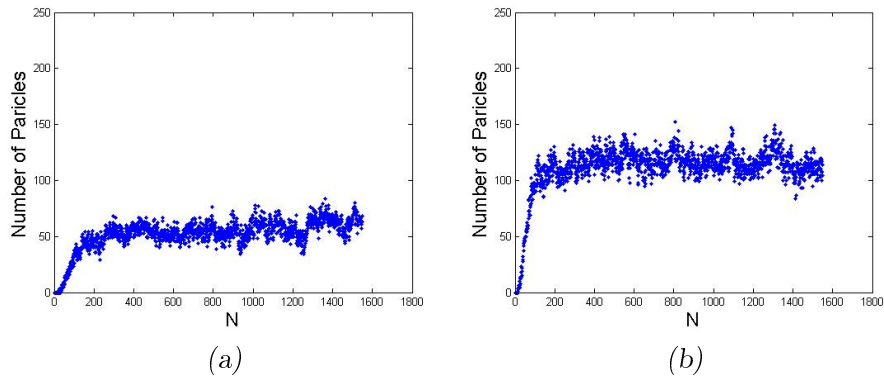


Fig. 4.19: The number of particle out of (a) inner side, and (b) outer side of the first layer boundaries versus number of resonance crossings for box3.

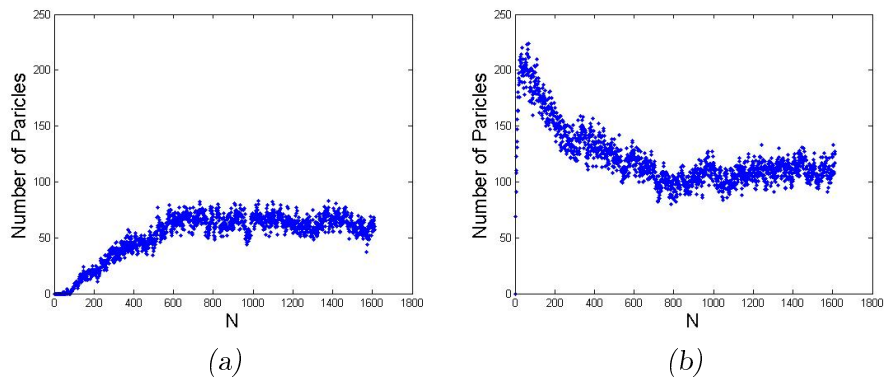


Fig. 4.20: The number of particle out of (a) inner side, and (b) outer side of the first layer boundaries versus number of resonance crossings for box4.

5. CONCLUSIONS

In the present thesis, we have shown that the jumps of adiabatic invariant not only happen when the trajectories pass through the resonance between first layer boundaries, but also happen in the domain between first and second layer boundaries where the resonance does not exist.

We show that multiple passages through the resonance lead to the destruction of the adiabatic invariability, and lead to the chaotic advection and mixing. We quantitatively demonstrated that the resultant mixing can be described by diffusion equation with flux-free boundary conditions. However, the boundary conditions need to be modified when the initial conditions are picked near first layer boundaries, in order to make the solution of the diffusion equation to match the numerical simulations of the system.

The first layer boundaries are not actual boundaries of the chaotic domain, while second layer boundaries are. We showed that there is a large number of particles transported between the domain inside first layer boundaries and the domain between first and second layer boundaries, but particles do not penetrate second layer boundaries. The distance between first and second layer boundaries not only depends on the size of the annulus, η , and the amplitude of the frequency oscillations, δ , but also depends on the magnitude of perturbation, ε . As ε decreases, for fixed value of η and δ , the distance between first and second layer boundaries decreases. And $\varepsilon \rightarrow 0$, first layer and second layer boundaries will overlap.

REFERENCES

- [1] S. H. Strogatz, “Nonlinear Dynamics and Chaos,” *Westview Press*, 2000.

- [2] J. Gleick, “Chaos-Making a new science,” *Viking*, 1987.

- [3] K. Bajer and H. K. Moffatt, “On a class of steady confined Stokes flows with chaotic streamlines,” *Journal of Fluid Mechanics*, vol.212, pp.337-363, 1990

- [4] A. I. Neishtadt, “Hamiltonian Systems with Three or More Degrees of Freedom,” *NATO ASI Series C*, vol.533, pp.193–213, 1999

- [5] T. H. Solomon and I. Mezic, “Uniform resonant chaotic mixing in fluid flows,” *Nature*, vol.425, pp.376–379, 2003.

- [6] D. L. Vainchtein, A. I. Neishtadt and L. M. Zelenyi, “Quasiadiabatic description of nonlinear particle dynamics in typical magnetotail configurations,” *Nonlinear Processes in Geophysics*, vol.12, pp.101–115, 2005.

- [7] E. N. Lorenz, “Deterministic Nonperiodic Flow,” *Journal of the Atmospheric Sciences*, vol.20, pp.130-141, 1963.

-
- [8] A. I. Neishtadt and A. Vasiliev, “Destruction of adiabatic invariance at resonances in slow-fast Hamiltonian systems,” *Nuclear Instruments and Methods in Physics Research A*, vol.561, pp.158–165, 2006.
- [9] D. L. Vainchtein, A. I. Neishtadt, and I. Mezic, “On passage through resonance in volume-preserving systems,” *Chaos*, vol.16, 043123, 2006.
- [10] H. Aref, “The development of chaotic advection,” *Physics of Fluids*, vol.14, pp.1315–1325, 2002.
- [11] D. Vainchtein, J. Widloski and R. O. Grigoriev, “Resonant mixing in perturbed action-action-angle flow,” *Physical Review*, vol.E78, 026302, 2008.
- [12] G. O. Fountain, D. V. Khakhar, I. Mezic and J. M. Ottino, “Chaotic mixing in a bounded three-dimensional flow,” *Journal of Fluid Mechanics*, vol.417, pp.265-301, 2000
- [13] D. L. Vainchtein, E. V. Rovinsky, L. M. Zelenyi, and A. I. Neishtadt, “Resonance and particle stochastization in nonhomogeneous electromagnetic fields,” *Journal of Nonlinear Science*, vol.14, pp.173–205, 2004
- [14] D. L. Vainshtein, A. A. Vasiliev, and A. I. Neishtadt, “Chaotic advection in a cubic Stokes flow,” *Physica D. Phenomena*, vol.111, pp.227-242, 1998

-
- [15] A. I. Neishtadt and A. A. Vasiliev, "Change of the adiabatic invariant at a separatrix in a volume-preserving 3D system," *Nonlinearity*, vol.12, pp.303-320, 1999
- [16] V. I. Arnol'd, "Proof of a Theorem of A. N. Kolmogorov on the Preservation of Conditionally Periodic Motions under a Small Perturbation of the Hamiltonian," *Russ. Math. Surv.*, vol.18, pp.13-40, 1963.
- [17] M. J. Feigenbaum, "Quantitative universality for a class of nonlinear transformations," *Journal of Statistical Physics*, vol.19, pp.25-52, 1978
- [18] J. A. Glazier, A. Libchaber, "Quasi-Periodicity and dynamical systems: An experimentalist's view," *IEEE Transactions on Circuits and Systems*, vol.35, NO.7, 1988

BIBLIOGRAPHY

Aref, H., "The development of chaotic advection," *Physics of Fluids*, vol.14, pp.1315–1325, 2002.

Arnol'd, V. I., "Proof of a Theorem of A. N. Kolmogorov on the Preservation of Conditionally Periodic Motions under a Small Perturbation of the Hamiltonian," *Russ. Math. Surv.*, vol.18, pp.13-40, 1963.

Bajer, K., and Moffatt, H. K., "On a class of steady confined Stokes flows with chaotic streamlines," *Journal of Fluid Mechanics*, vol.212, pp.337-363, 1990

Feigenbaum, M. J., "Quantitative universality for a class of nonlinear transformations," *Journal of Statistical Physics*, vol.19, pp.25-52, 1978

Fountain, G. O., Khakhar, D. V., Mezic, I., and Ottino, J. M., "Chaotic mixing in a bounded three-dimensional flow," *Journal of Fluid Mechanics*, vol.417, pp.265-301, 2000

Glazier, J. A., and Libchaber, A., "Quasi-Periodicity and dynamical systems: An experimentalist's view," *IEEE Transactions on Circuits and Systems*, vol.35, NO.7, 1988

Gleick, J., "Chaos-Making a new science," *Viking*, 1987.

Lorenz, E. N., "Deterministic Nonperiodic Flow," *Journal of the Atmospheric Sciences*, vol.20, pp.130-141, 1963.

Neishtadt, A. I., "Hamiltonian Systems with Three or More Degrees of Freedom," *NATO ASI Series C*, vol.533, pp.193–213, 1999

Neishtadt, A. I., and Vasiliev, A. A., "Change of the adiabatic invariant at a separatrix in a volume-preserving 3D system," *Nonlinearity*, vol.12, pp.303-320, 1999

Neishtadt, A. I., and Vasiliev, A. A., "Destruction of adiabatic invariance at resonances in slow-fast Hamiltonian systems," *Nuclear Instruments and Methods in Physics Research A*, vol.561, pp.158–165, 2006.

Solomon, T. H., and Mezic, I., "Uniform resonant chaotic mixing in fluid flows," *Nature*, vol.425, pp.376–379, 2003.

Strogatz, S. H., "Nonlinear Dynamics and Chaos," *Westview Press*, 2000.

Vainchtein, D. L., Neishtadt, A. I., and Mezic, I., "On passage through resonance in volume-preserving systems," *Chaos*, vol.16, 043123, 2006.

Vainchtein, D. L., Neishtadt, A. I., and Zelenyi, L. M., “Quasiadiabatic description of nonlinear particle dynamics in typical magnetotail configurations,” *Nonlinear Processes in Geophysics*, vol.12, pp.101–115, 2005.

Vainchtein, D. L., Rovinsky, E. V., Zelenyi, L. M., and Neishtadt, A. I., “Resonance and particle stochastization in nonhomogeneous electromagnetic fields,” *Journal of Nonlinear Science*, vol.14, pp.173–205, 2004

Vainshtein, D. L., Vasiliev, A. A., and Neishtadt, A. I., “Chaotic advection in a cubic Stokes flow,” *Physica D. Phenomena*, vol.111, pp.227-242, 1998

Vainchtein, D., Widloski, J., and Grigoriev, R. O., “Resonant mixing in perturbed action-action-angle flow,” *Physical Review*, vol.E78, 026302, 2008.